

NUMERICAL STUDY OF BOND BEHAVIOR IN SINGLE-LAP SHEAR TEST AT MESO-SCALE

Y. WANG*, J. VOREL[†], C. CARLONI[‡], J. BELIS[§] AND R. WAN-WENDNER[¶]

* Magnel-Vandepitte Laboratory, Department of Structural Engineering and Building Materials, Ghent University
Technologiepark-Zwijnaarde 60, Ghent, 9052, Belgium
e-mail: yilin.wang@ugent.be, www.ugent.be

[†]Department of Mechanics, Faculty of Civil Engineering, Czech Technical University in Prague
Thákurova 7, Praha 6, Prague, 16629, Czech Republic
e-mail: jan.vorel@fsv.cvut.cz, www.cvut.cz

[‡]Department of Civil and Environmental Engineering, Case Western Reserve University
10900 Euclid Ave, Cleveland, 44107, USA
e-mail: cxc966@case.edu, www.case.edu

[§]Magnel-Vandepitte Laboratory, Department of Structural Engineering and Building Materials, Ghent University
Technologiepark-Zwijnaarde 60, Ghent, 9052, Belgium
e-mail: jan.belis@ugent.be, www.ugent.be

[¶]Magnel-Vandepitte Laboratory, Department of Structural Engineering and Building Materials, Ghent University
Technologiepark-Zwijnaarde 60, Ghent, 9052, Belgium
e-mail: roman.wanwendner@ugent.be, www.ugent.be

Key words: Meso-scale Simulation, Bond Behavior, Lattice Discrete Particle Model (LDPM), Width Effect, Concrete

Abstract. The use of fiber-reinforced polymer (FRP) for strengthening concrete structures has gained significant interest. Given that the challenges and limitations of experimental investigations, numerical modeling is essential for studying FRP-reinforced concrete structures. However, simulating FRP-concrete debonding failure is challenging due to the complex nature of concrete damage, which often involves a thin layer of concrete substrate debonding with the FRP strip. This study investigates the bond behavior between steel-reinforced polymer (SRP) strip and concrete using a three-dimensional (3D) meso-scale lattice discrete particle model (LDPM). The model accounts for the inherent heterogeneity of concrete, including the distribution of coarse aggregates, and simulates the macroscopic debonding process as a propagating fracture inside the concrete substrate. In this research, the LDPM is calibrated and validated against experimental data and incorporates a meso-scale representation of concrete with SRP treated as a linear elastic material. This study investigates the bond behavior in single-lap shear tests, focusing on the load response and the initiation and propagation of cracks at the concrete substrate. A series of parametric studies were conducted to examine the width effect and the influence of the minimum modelled concrete coarse aggregate. The numerical simulations offer valuable insights into the mechanics of SRP-concrete interactions.

1 INTRODUCTION

During the service life of concrete structures, the mechanical properties of concrete deteriorate, necessitating efficient and cost-effective strengthening methods over demolition and reconstruction. Externally bonded fiber-reinforced polymers (EB-FRPs) have emerged as a widely used solution due to their lightweight and high-strength properties, improving the performance of existing structures [1].

The bond between FRP and concrete substrate is critical for transferring stresses in a EB-FRP system. Laboratory tests, such as single/double-lap shear [2–5] and flexural beam tests [6, 7], are commonly used to study the FRP-concrete bond behavior under service conditions, considering factors like substrate preparation, bonded length and width, and environmental conditions. While studies have explored the mixed-mode I/II [8, 9] failure mechanisms, involving both shear and normal debonding, limited research exists on the bond behavior in the critical debonding mechanisms.

Numerical modeling provides a powerful tool for understanding the debonding mechanisms in single/double-lap shear and flexural beam tests. Typically, macro-scale modeling simplifies the failure of FRP-strengthened concrete structures by treating the FRP-concrete interface behavior as occurring in the cohesive elements between FRP and concrete [10–12]. However, experimental observations consistently show that failure often occurs within the concrete substrate [2]. To better capture this behavior, a meso-scale modeling approach is required. This approach considers the heterogeneous nature of concrete and more accurately represents the mixed-mode I/II debonding mechanisms at the FRP-concrete interface. While meso-scale models have been applied to FRP-strengthened concrete elements, their application to the bond behavior in single/double-lap shear and flexural beam tests remains limited. Zhang et al. [13] and Wang et al. [14] advanced finite element modeling (FEM) techniques by explicitly defining the individual

components of concrete, including aggregates, mortar, and the aggregate-mortar interface. The initiation and propagation of damage within the mortar and cracking at the mortar-aggregate interface during the FRP debonding process was captured. However, incorporating realistic aggregate size and fraction into these models demands significant computational resources, presenting a challenge for broader implementation.

More detailed models that account for the internal heterogeneity of concrete are essential for accurately capturing its behavior. This study employs the lattice discrete particle model (LDPM), which represents concrete's internal structure as an assemblage of coarse aggregate pieces interacting at discrete interfaces [15]. The LDPM effectively models heterogeneity and facilitates the simulation of structural breakups and fragmentation under various loading conditions [16–20].

This study investigates the debonding mechanism of steel-reinforced polymer (SRP)-concrete interfaces in a single-lap shear test using numerical approaches. A three-dimensional (3D) model of the single-lap shear test was developed based on LDPM for the concrete domain, with calibration and validation performed through comparisons with experimental data that is described in ASTM standard [21]. A subsequent parametric study examined the influence of bonded width and aggregate size on the bond behavior of the SRP-concrete interface.

2 OVERVIEW OF EXPERIMENTAL CAMPAIGN

This section provides a concise review of the experimental studies on single-lap shear and flexural beam tests of SRP-concrete joints, as detailed in [5]. It summarizes the materials and test setups used for the numerical modeling presented in subsequent sections.

All concrete specimens, including those for single-lap shear, flexural notched beam tests, and material characterization, were cast from a single batch of normal-weight concrete with a maximum aggregate size of 15 mm. Compres-

sive strength was measured over 420 days using 150 mm cube specimen, with fitted strength-time functions used to estimate properties at 300 days. This time is corresponding to the time frame when SRP strips were applied on the concrete surface 300 days after casting. The compressive strength at the time of testing was interpolated between available test results as 30.8 MPa. The peak load of the flexural beam test on a notched specimen (600 × 150 × 150 mm) was recorded as 8.3 kN. The average elastic modulus and tensile strength of the SRP strip, based on the fiber area, were 258 GPa and 3060 MPa, respectively. The global elastic modulus of the composite strip can be calculated as follows:

$$E_f = \frac{E_s \cdot t_s}{t_f} = 16.4 \text{ GPa} \quad (1)$$

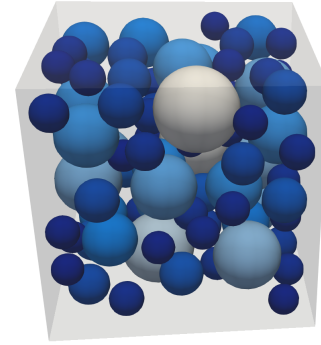
in which $t_s = 0.254 \text{ mm}$ is the equivalent thickness of the steel fibers, $t_f = 4 \text{ mm}$ is the nominal thickness of the composite strip, and E_s is the elastic modulus of the steel fibers.

The classical push-pull configuration was used for the single-lap shear test, with the SRP pulled while the concrete prism was restrained. Each concrete prism measured 150 mm in width and depth and 600 mm in length. Epoxy resin impregnated the fibers across the entire SRP strip. The SRP strip had a nominal total thickness of 4 mm. Bonding began 70 mm from the loaded end of the strip to create an initial interfacial notch. The bonded length and width is 300 mm and 75 mm, respectively. Two linear variable differential transformers (LVDTs) were mounted on the concrete surface near the top edge of the bonded region. The global slip, denoted as g , was defined as the average displacement recorded by these two LVDTs [5].

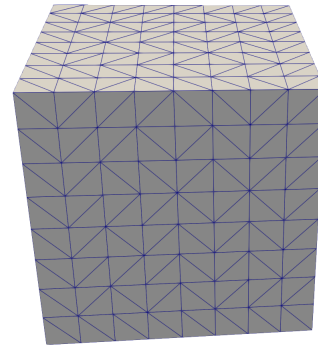
3 MESO-SCALE MODELLING

3.1 Lattice discrete particle model (LDPM)

In this study, the lattice discrete particle model (LDPM), developed by Cusatis et al. [15], was utilized to represent concrete behavior at the meso-scale.



(a)



(b)



(c)

Figure 1: (a) Particle system, (b) tetrahedralization and (c) facets of tessellation for a prism specimen.

3.1.1 Geometrical characterization

To construct the concrete mesostructure, coarse aggregate particles were randomly distributed within the geometric volume of the specimen using a try-and-reject algorithm, as illustrated in Figure 1a. The fuller coefficient n_F governs its optimal packing properties. The Delaunay tetrahedralization method was employed to create a 3D network of tetrahedra. This

approach utilizes the coordinates of the particle centers as input and produces a volumetric mesh as output (see Figure 1b). A tessellation with 12 triangular facets was generated within each tetrahedron by linking edge-points, face-points, and tet-points. These facets served as potential locations for material failure (see Figure 1c). It should be noted that the aggregate were assumed to be a non-damaged material in the model.

3.1.2 Constitutive law

In the meso-scale model, a constitutive law is assigned to each facet, and equilibrium is imposed using the principle of virtual work. The elastic behavior assumes normal and shear stresses are proportional to the corresponding strains:

$$\sigma_N = E_N \varepsilon_N; \sigma_M = E_T \varepsilon_M; \sigma_L = E_T \varepsilon_L \quad (2)$$

where N , M , and L correspond to the normal direction and two perpendicular tangent directions in each facet. $E_N = E_0$ (effective normal modulus) and $E_T = \alpha E_0$ (α is shear-normal coupling parameter). These are related to the macroscopic Young's modulus E and Poisson's ratio ν as: $E_0 = E/(1 - 2\nu)$ and $\alpha = (1 - 4\nu)/(1 + \nu)$.

Beyond the elastic behavior, the LDPM constitutive equations incorporate fracture and softening in tension, material compaction and pore collapse in compression, and frictional effects.. For fracturing, the effective strain and stress are defined as:

$$\begin{aligned} \varepsilon &= \sqrt{\varepsilon_N^2 + \alpha(\varepsilon_M^2 + \varepsilon_L^2)} \\ \sigma &= \sqrt{\sigma_N^2 + (\sigma_M^2 + \sigma_L^2)}/\alpha \end{aligned} \quad (3)$$

with stresses expressed as:

$$\sigma_N = \sigma \frac{\varepsilon_N}{\varepsilon}; \sigma_M = \sigma \frac{\alpha \varepsilon_M}{\varepsilon}; \sigma_L = \sigma \frac{\alpha \varepsilon_L}{\varepsilon} \quad (4)$$

The effective stress σ evolves elastically ($\dot{\sigma} = E_0 \dot{\varepsilon}$) up to a boundary $\sigma_{bt}(\varepsilon, \omega)$, defined as:

$$\sigma_{bt}(\varepsilon, \omega) = \sigma_0(\omega) \exp \left[-H_0(\omega) \frac{\langle \varepsilon_{\max} - \varepsilon_0(\omega) \rangle}{\sigma_0(\omega)} \right] \quad (5)$$

where σ_ω depends on the tensile and shear strengths (σ_t and σ_s):

$$\begin{aligned} \sigma_0(\omega) &= \sigma_t \frac{-\sin(\omega)}{2\alpha \cos^2(\omega)/r_{st}^2} \\ &+ \frac{\sqrt{\sin^2(\omega) + 4\alpha \cos^2(\omega)/r_{st}^2}}{2\alpha \cos^2(\omega)/r_{st}^2} \end{aligned} \quad (6)$$

The softening modulus $H_0(\omega)$ follows a power function of ω : $H_0(\omega) = H_t(2\omega/\pi)^{n_t}$, where H_t is the pure tension softening modulus and n_t is the positive softening exponent.

Compression is limited by a strain-hardening boundary σ_{bc} , dependent on volumetric strain (ε_V) and deviatoric strain (ε_D), to capture the pore collapse and material compaction.

Frictional effects under compressive stress are modeled via incremental plasticity, with plastic strain increments:

$$\begin{aligned} \dot{\varepsilon}_M^p &= \dot{\lambda} \partial \varphi / \partial \sigma_M \\ \dot{\varepsilon}_L^p &= \dot{\lambda} \partial \varphi / \partial \sigma_L \end{aligned} \quad (7)$$

where the plastic potential is $\varphi = \sqrt{\sigma_M^2 + \sigma_L^2} - \sigma_{bs}(\sigma_N)$. The shear strength σ_{bs} follows a non-linear frictional law:

$$\begin{aligned} \sigma_{bs}(\sigma_N) &= \sigma_s + (\mu_0 - \mu_\infty) \sigma_{N0} - \mu_\infty \sigma_N \\ &- (\mu_0 - \mu_\infty) \sigma_{N0} \times \exp(\sigma_N / \sigma_{N0}) \end{aligned} \quad (8)$$

where μ_0 and μ_∞ are the initial and final friction coefficients, and σ_{N0} is the transition normal stress for the range of μ_0 to μ_∞ .

3.2 Calibration

The calibration of the LDPM model can be achieved by comparing numerical results with experimental data from compression tests and flexural beam tests [5]. The meso-scale modeling was employed, as depicted in Figure 2, in which the calibration results were also shown. It can be found that the compressive strength and load-crack mouth opening displacement (CMOD) response of the flexural beam test demonstrate strong agreement between numerical simulations and experimental data. The calibrated parameters used in the model are summarized in Table 1.

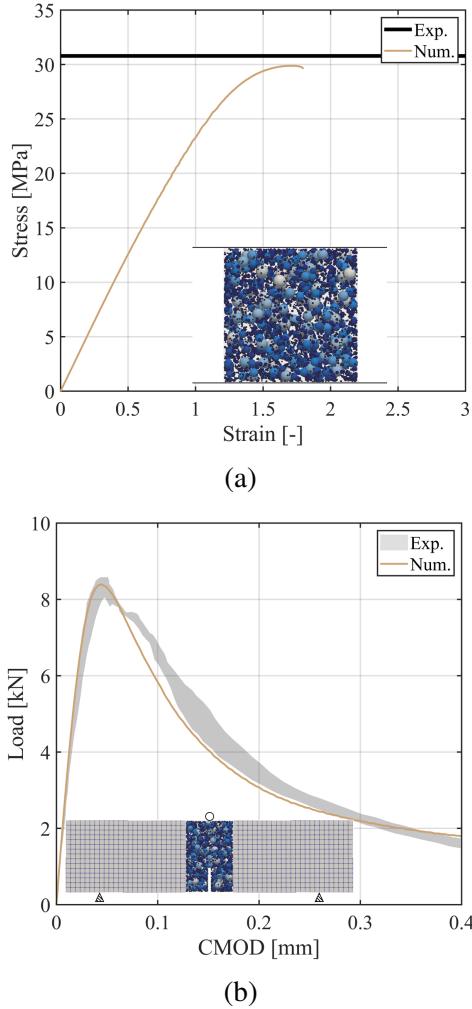


Figure 2: Calibrations for (a) compression test and (b) flexural beam test.

3.3 Modelling of single-laps shear test

Following the experimental study [5], the meso-scale model geometry is illustrated in Figure 3. The FRP strip (bonded) was represented with quadrilateral shell elements and bonded to the concrete prism, assuming a perfect connection (master-slave approach) without the need for interface elements. For the steel components in the test setup, including the top and bottom plates as well as the four connecting bars, FEM was applied. The connections between the bars and bottom plate were defined using a master-slave approach. Frictional contact was used to simulate the interaction between the concrete prism and top plate. The steel material was treated as purely elastic

in the simulations.

4 Comparison with experimental results in the literature

Figure 4 compares the numerical and experimental load responses for the single-lap shear test with bonded width of 75 mm. The numerically predicted average plateau load P_{crit} (as defined in [5]) is 19.36 kN, which deviates from the experimental result (20.57 kN) by 5.88%. It should be noted that three simulations with three different sets of random particle placements (meso-structures), were considered to obtain the LDPM response. The numerical results closely align with the experimental data, though the initial stiffness in the simulations is slightly higher. This discrepancy may stem from a potential rotation of the aluminum plate during the experiments, which was not accounted for in this simulation. Such rotation, caused by the eccentricity between the LVDT contact point and the SRP strip surface, could have influenced the LVDT readings and led to a minor variation in the initial slope of the experimental load response, explaining the observed difference in initial stiffness.

Table 1: LDPM parameters.

Parameters	Value	Unit
Min.aggregate	1.6	mm
Max.aggregate	15	mm
Fuller coefficient	0.5	-
Normal modulus	42500	MPa
Alpha	0.25	-
Tensile strength	2.64	MPa
Tensile characteristic length	255	mm
Softening exponent	0.8	-
Shear strength ratio	3.4	-
Initial friction	0.05	-
Initial hardening modulus ratio	0.2	-
Transitional strain ratio	4	-
Deviatoric strain threshold ratio	1	-
Deviatoric damage parameter	5	-
Transitional stress	600	MPa
Asymptotic friction	0	-
Volumetric deviatoric coupling	0	-



Figure 3: Meso-scale modelling of the single-lap shear test.

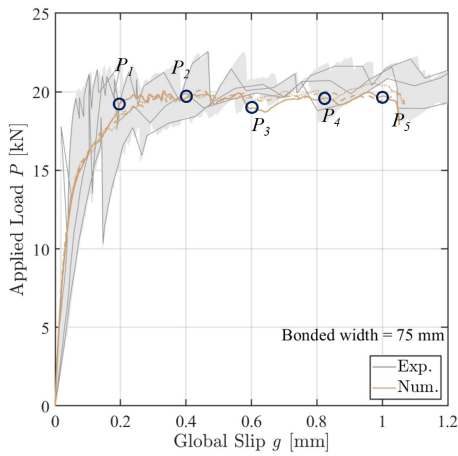


Figure 4: Experimental and numerical load responses.

Figure 5 illustrates the evolution of concrete substrate failure from the loaded end to the free end at 5 points for one simulation (see Figure 4) along the load-slip curve. Initially, damage concentrates near the loaded end. At a global slip of 0.1 mm, the stiffness begins to decrease. As displacement increases from 0.2 mm (P_1) to 1 mm (P_5), the SRP strip gradually peels off, and

the damage propagates along the bonded length toward the free end. Moreover, the crack progresses inside the concrete along a horizontal path and eventually spreads beneath the SRP-bonded area, causing debonding of a thin concrete substrate layer. This phenomenon will be discussed in detail in the following section.

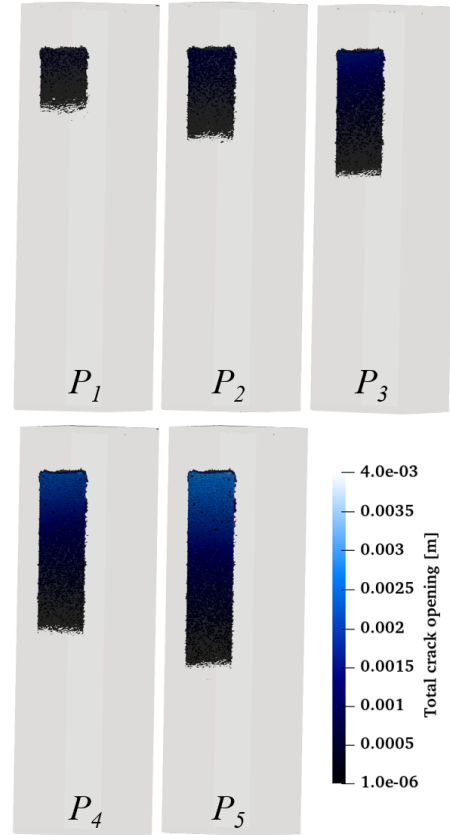


Figure 5: Numerical concrete failure patterns.

5 PARAMETRIC STUDY

5.1 Bonded width

A numerical analysis was conducted on single-laps shear tests with different bonded widths (15 mm, 30 mm, 40 mm, 50 mm, 75 mm, and 90 mm). Figure 6 illustrates the load responses in the meso-scale model for different bonded widths. As the bonded width increases, the plateau load shows obvious increases. Figure 7 presents the relationship between the plateau load per unit width P_{crit}/b_f and width ratio b_f/b of SRP and concrete. P_{crit} is determined when the load-slip curve reaches the plateau. The points represent the average

values of b_f/b from three simulations for each width case. As the width ratio increases, the plateau load per unit width gradually decreases before stabilizing.

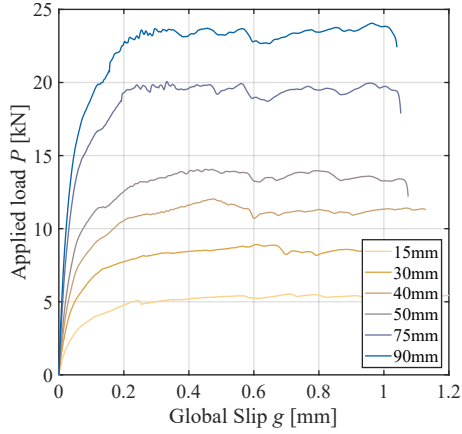


Figure 6: Effect of bonded width on load response.

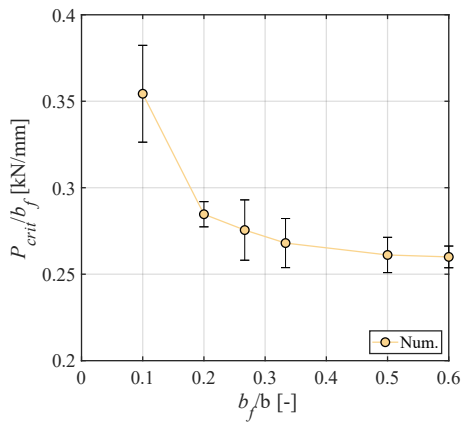


Figure 7: Plateau load per unit width.

5.2 Aggregate size

To study the effect of aggregate size on the bond behavior of SRP-concrete interface, three minimum aggregate sizes ($d_0 = 1.6$ mm, 3.6 mm, and 5.6 mm) were selected for the meso-scale modelling of the single-lap shear test. The maximum aggregate size remains 15 mm for all cases. Figure 8 compares the plateau load of the single-lap shear test simulated with three minimum aggregate sizes. The results indicate that the plateau load increases as the minimum aggregate size becomes larger. This trend is further explained by the failure patterns shown in

Figure 9, which depict the side views of the meso-scale models for various aggregate sizes. Larger minimum aggregate sizes led to greater failure depths t_d in the concrete substrate, as the cracks propagated through longer paths around the aggregates. This crack bypassing process requires more energy, increasing the overall bond capacity. Consequently, simulated samples with larger minimum particle size provide larger estimates of bond capacity.

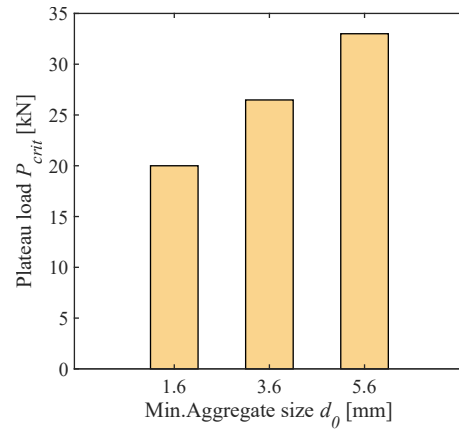


Figure 8: Effect of aggregate size on load response.

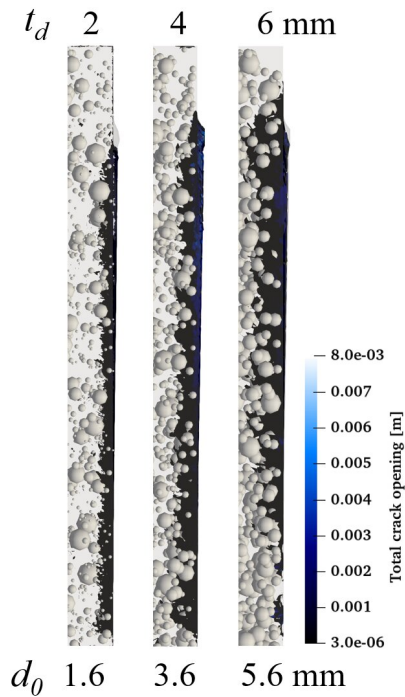


Figure 9: Effect of aggregate size on failure pattern.

6 CONCLUSIONS

This study investigated the bond behavior of the SRP-concrete interface based a single-lap shear test simulation. A realistic 3D meso-scale concrete structure was generated using the lattice discrete particle model. The numerical results, including load–slip curves, bond capacity, and failure propagation patterns have been analyzed. A series of parametric studies about the bonded width and aggregate size were executed. The main conclusions are presented as follows:

- The 3D meso-scale model effectively simulates concrete damage during SRP strip debonding, capturing the thin damage layer at the concrete substrate close to the bonded interface. Validation against experimental data showed good agreement.
- A larger bonded width results in an overall increase in plateau load, as the greater surface area provides more capacity for load transfer between the SRP and concrete. However, as the width ratio increases, the plateau load per unit width gradually decreases and eventually levels off.
- Simulations with larger minimum aggregate sizes revealed a deeper failure inside the concrete substrate. This increased failure depth absorbs more energy, thereby enhancing bond capacity.

REFERENCES

- [1] Xinyan Guo, Peiyan Huang, Yilin Wang, Shenyunhao Shu, and Xiaohong Zheng. Flexural performance of reinforced concrete beams strengthened with carbon fiber-reinforced polymer (CFRP) under hygrothermal environment considering the influence of cfrp–concrete interface. *Acta Mechanica Solida Sinica*, 34:381–392, 2021.
- [2] Yilin Wang, Chihui Huang, and Xinyan Guo. Study on the influence of end anchoring on CFRP-concrete interface through double-lap shear testing. *Structures*, 69:107457, 2024.
- [3] Wen Li, Peiyan Huang, Zhanbiao Chen, Xiaohong Zheng, Yi Yang, and Xinyan Guo. Bond behavior of fully bonded CFRP-concrete interface with improved double shear tests. *Journal of Building Engineering*, 43:102866, 2021.
- [4] Yilin Wang and Xinyan Guo. Experimental investigation on bond behavior of cfrp-concrete interface with end anchorage in hygrothermal environments. *Journal of Building Engineering*, 68:106141, 2023.
- [5] Christian Carloni, Mattia Santandrea, and Imohamed Ali Omar Imohamed. Determination of the interfacial properties of srp strips bonded to concrete and comparison between single-lap and notched beam tests. *Engineering Fracture Mechanics*, 186:80–104, 2017.
- [6] Mohammad Reza Esfahani, MR Kianoush, and AR Tajari. Flexural behaviour of reinforced concrete beams strengthened by CFRP sheets. *Engineering structures*, 29(10):2428–2444, 2007.
- [7] Mand Kamal Askar, Ali Falyeh Hassan, and Yaman SS Al-Kamaki. Flexural and shear strengthening of reinforced concrete beams using frp composites: A state of the art. *Case Studies in Construction Materials*, 17:e01189, 2022.
- [8] Md Shah Alam, Toshiyuki Kanakubo, and Akira Yasojima. Shear-peeling bond strength between continuous fiber sheet and concrete. *ACI Structural Journal*, 109(1), 2012.
- [9] Francesco Focacci, Mohammad Minhajur Rahman, Tommaso D’Antino, and Christian Carloni. Frp strips externally bonded to quasi-brittle substrates: Discussions

- and advances of open research topics. *Journal of Composites for Construction*, 28(6):04024055, 2024.
- [10] GM Chen, JF Chen, and JG Teng. Behaviour of frp-to-concrete interfaces between two adjacent cracks: A numerical investigation on the effect of bondline damage. *Construction and building materials*, 28(1):584–591, 2012.
- [11] Justas Slaitas and Juozas Valivonis. Bond strength evaluation methods of rc members strengthened with frp composites. *Engineering Structures*, 249:113357, 2021.
- [12] Miao Su, Hui Peng, Ming Yuan, and Shaofan Li. Identification of the interfacial cohesive law parameters of frp strips externally bonded to concrete using machine learning techniques. *Engineering Fracture Mechanics*, 247:107643, 2021.
- [13] Zihua Zhang, Tianlin Zhao, and Xuan Wang. Mesoscale modelling of concrete damage in frp-concrete debonding failure. *Engineering Structures*, 289:116310, 2023.
- [14] Xuan Wang, Tianlin Zhao, Jialong Guo, Zihua Zhang, and Xiaogang Song. Mesoscale modelling of the frp-concrete debonding mechanism in the pull-off test. *Composite Structures*, 309:116726, 2023.
- [15] Gianluca Cusatis, Daniele Pelessone, and Andrea Mencarelli. Lattice discrete particle model (ldpm) for failure behavior of concrete. i: Theory. *Cement and Concrete Composites*, 33(9):881–890, 2011.
- [16] Gianluca Cusatis, Andrea Mencarelli, Daniele Pelessone, and James Baylot. Lattice discrete particle model (ldpm) for failure behavior of concrete. ii: Calibration and validation. *Cement and Concrete Composites*, 33(9):891–905, 2011.
- [17] Yilin Wang, Gilda Daissé, Mattia Santandrea, Marco Marcon, Jan Vorel, Roman Wan-Wendner, and Christian Carloni. Simulation of bond behavior of frp-concrete joints using lattice discrete particle model. *Journal of Composites for Construction*, pages doi:10.1061/JCCOF2/CCENG-4693, 2025.
- [18] Sina Khodaie, Fabio Matta, and Mohammed Alnaggar. Discrete meso-scale modeling and simulation of shear response of scaled glass frp reinforced concrete beams without stirrups. *Engineering Fracture Mechanics*, 216:106486, 2019.
- [19] Mohammed Abdellatef, Jan Vorel, Roman Wan-Wendner, and Mohammed Alnaggar. Predicting time-dependent behavior of post-tensioned concrete beams: discrete multiscale multiphysics formulation. *Journal of Structural Engineering*, 145(7):04019060, 2019.
- [20] Jan Vorel, Marco Marcon, Gianluca Cusatis, Ferhun Caner, Giovanni Di Luzio, and Roman Wan-Wendner. A comparison of the state of the art models for constitutive modelling of concrete. *Computers & Structures*, 244:106426, 2021.
- [21] ASTM D8337/D8337M-21-Standard Test Method for Evaluation of Bond Properties of FRP Composite Applied to Concrete Substrate using Single-Lap Shear Test. Standard, January 2021.